Tropical Pacific warming patterns influence future hydroclimate shifts and extremes in the Americas

Ulla K. Heede[1*], Nathan Lenssen[2,3,4], Kristopher B. Karnauskas[1,2] and Clara Deser[4]

[1] *Cooperative Institute for Research in Environmental Sciences, University of Colorado, Boulder, CO, USA*
[2] *Department of Atmospheric and Oceanic Sciences, University of Colorado, Boulder, CO, USA*
[3] *Department of Applied Mathematics and Statistics, Colorado School of Mines, Golden, CO, USA*
[4] *NSF National Center for Atmospheric Research, Boulder, CO, USA*

Abstract

The eastern tropical Pacific (ETP) Ocean is projected to warm faster than the Atlantic or Indian Oceans in the 21st century, yet this prediction is highly uncertain due to model-observation discrepancies. The potential impacts of this uncertainty on regional terrestrial hydroclimates are largely unknown, which is problematic for climate risk assessments. To address this, we designed novel atmospheric model experiments simulating future global warming with and without enhanced ETP warming, superimposed upon an idealized El Niño-Southern Oscillation (ENSO) cycle. Our results show that enhanced ETP warming significantly influences future terrestrial hydroclimates in several regions across the tropical and subtropical Americas. In southern Mexico, Central America and the Amazon region, enhanced ETP warming exacerbates long term drought trends and extreme drought events, yet the opposite is true in south-central South America. Along the west coast of the continental western United States, the effects of enhanced ETP warming manifest as El Niño-related extreme precipitation anomalies. These findings illustrate how climate impact projections may be misrepresented in conventional multi-model analysis, which does reflect true uncertainty of the future tropical Pacific warming pattern.

* Corresponding Author: Ulla K. Heede, 4001 Discovery Dr, Boulder, Colorado, ulla.heede@colorado.edu

Plain Language Summary

The tropical Pacific responds to global warming is uncertain, particularly because models and observations do not agree over the past decades. Models simulate an enhanced warming of the eastern tropical Pacific, yet observations show the opposite trend. This uncertainty may propagate into uncertainty in regional precipitation patterns, which have consequences for society's ability to adapt to climate change. We designed two model experiments with (EP) and without (noEP) enhanced eastern tropical Pacific warming to understand how ocean warming patterns affect precipitation in the Americas. We found that droughts were intensified in Central America and the Amazon region in the EP experiment compared to the noEP experiment (i.e., when the tropical Pacific warms up faster, droughts intensify in those regions), yet reduced in south-central South America. We also looked at changes to extreme events and found that d El Niño-related drought extremes were exacerbated more in the EP relative to the noEP experiment in the Amazon, and wet extremes were exacerbated in the Western U.S. These results show how the uncertainty in future ocean warming patterns can propagate into uncertainty in terrestrial precipitation trends and changes to extremes. This finding has consequences for society's ability to adapt to future climate change.

Key Points:

1. Uncertainty in the future tropical Pacific warming pattern propagates into future changes to terrestrial hydroclimates.

2. Enhanced eastern Pacific warming, as simulated by models, exacerbates droughts in Central America and the Amazon region.

3. Extreme precipitation events occurring in several regions during El Niño years are modulated by the background Pacific warming pattern.

Introduction

Precipitation variability is one of the most societally impactful aspects of contemporary climate, yet it remains one of the most difficult to predict. Persistent droughts can alter regional biomes (Vicente-Serrano *et al.*, 2013) and short term extreme drought or flooding events can impose severe challenges for agriculture (Devereux, 2007; Watanabe *et al.*, 2018), water management (Crochemore, Ramos and Pappenberger, 2016), human health (Harp *et al.*, 2021; Buchwald *et al.*, 2022), natural hazard safety (Nadim *et al.*, 2006; Hong *et al.*, 2007) and economic production (Kotz et al., 2022). Despite the importance of understanding precipitation changes for successful adaption to climate change, projecting the response of precipitation to anthropogenic radiative forcing is among our greatest scientific challenges.

Some aspects of the hydrological response to global warming are robust, such as the global increase in water vapor following the Clausius-Clapeyron relation, which in turn is shown to increase precipitation and evaporation rates by 2% per degree warming on average (Held and Soden, 2006). However, this scaling estimate is global and does not specify where precipitation increases take place. Assuming a static background state of moisture transport and convergence, a framework of 'wet gets wetter' has been proposed. In this framework, areas of global moisture convergence and net positive precipitation minus evaporation (P-E) such as the tropics receive more precipitation. Conversely, areas of moisture divergence and negative P-E experience increased drought (Manabe and Wetherald, 1975; Allen and Ingram, 2002; Wetherald and Manabe, 2002; Chou and Neelin, 2004; Held and Soden, 2006).

However, several studies have shown that observed precipitation trends are not consistent with the wet-gets-wetter framework, particularly over land (Xie *et al.*, 2010; Greve *et al.*, 2014; Pfahl, O'Gorman and Fischer, 2017). The wet-gets-wetter paradigm stems from the supposition of spatially homogeneous changes in surface temperature that disregards the geographically varying warming of the Earth's surface under external forcing. The circulation alterations that such temperature gradients create have the potential to influence the regional precipitation response. In general, land warms faster than the sea surface, polar regions warm faster than the subtropics, and the Northern Hemisphere has warmed more than the Southern Hemisphere over the industrial era (Lenssen *et al.*, 2019; Gulev *et al.*, 2021; Morice *et al.*, 2021). In addition, the ocean has experienced heterogeneous warming rates throughout the observational record as the subpolar North Atlantic, the east/central equatorial Pacific and the Southern Ocean show flat or cooling trends in recent decades (Dong and Lu, 2013; Keil *et al.*, 2020; Dong *et al.*, 2022), yet the Indian Ocean has experienced accelerated warming since 1950 (Hu and Fedorov, 2019; Zhang *et al.*, 2019). These unequal warming rates cause anomalous surface temperature gradients which in turn alter the large-scale atmospheric circulation and ultimately the transport and convergence of moisture and subsequent precipitation.

The future pattern of sea surface temperature (SST) changes in the tropical Pacific is of particular concern as this region contains the largest convective zone on the planet and has been widely recognized as a key driver of global weather and climate variability as early as the 1920s (Walker, 1925). More recently the radiative response to surface warming in the western tropical Pacific has been identified as a key driver of global climate sensitivity (Dong *et al.*, 2019; Bloch-Johnson *et al.*, 2024). Yet, the response of the tropical Pacific to anthropogenic radiative forcing is uncertain (DiNezio, Clement and Vecchi, 2010; Seager *et al.*, 2019; Heede and Fedorov, 2021; Wills *et al.*, 2022). Over the satellite era (i.e., since the 1980s), the eastern tropical Pacific has experienced a lack of warming, but adjacent ocean regions have warmed, resulting in accelerated trade winds along the equatorial Pacific (Dong and Lu, 2013; Kosaka and Xie, 2013; Heede and Fedorov, 2023a). This multi-decadal trend is thought to be a combination of natural variability, a transient response to greenhouse gas forcing (typically dubbed the 'ocean dynamical thermostat' mechanism: (Clement *et al.*, 1996; Sun and Liu, 1996; Heede, Fedorov and Burls, 2020; Heede and Fedorov, 2023a; Jiang *et al.*, 2024), anthropogenic aerosols (Hwang *et al.*, 2024; Watanabe *et al.*, 2024) and Southern Ocean cooling (Dong *et al.*, 2022; Kang *et al.*, 2023). However, such a trend pattern is rarely captured by historical simulations from global coupled climate models (Seager et al., 2022; Wills *et al.*, 2022). That is, models predict an enhanced eastern Pacific warming emerging in the 21st century (Heede and Fedorov, 2021; Wu *et al.*, 2021; Ying *et al.*, 2022) and this is argued to be caused by a slowdown of tropical circulation (Vecchi and Soden, 2007) and in the oceanic subtropical cells (Heede, Fedorov and Burls, 2020). Whether and when the observed trend will reverse and an enhanced eastern Pacific warming emerge is uncertain given the inability of the same models to capture the observed trends. Overall, this uncertainty hinders robust projections of global dynamical changes driven by tropical Pacific warming trends and limits our ability to understand the full potential spectrum of future rainfall projections with consequences for societal adaptation.

While the sensitivity of precipitation trends in the Americas to Pacific warming patterns has been investigated in general (Seager and Vecchi, 2010), the consequences of the current model-observational discrepancy have not been quantitatively investigated from a climate impacts focused perspective. As studies have considered large-scale climatic and precipitation responses to various ocean warming patterns in the tropical Pacific (Zhang *et al.*, 2019; Fosu, He and Liguori, 2020), much less attention has been paid to the terrestrial and regional precipitation responses, which is more important for assessing climate impacts. The agreement on enhanced eastern Pacific warming in CMIP6 models means that the spread among models, and the resulting science using these models, does not capture the true uncertainty associated with the tropical Pacific warming response with perilous consequences for society's ability to plan for a wider range of possible future hydroclimatic changes.

An ubiquitous challenge in projecting precipitation is that precipitation is highly variable across space and time (Meehl, Wheeler and Washington, 1994; Pendergrass *et al.*, 2017; He and Li, 2019; Schwarzwald *et al.*, 2021). For many human and natural systems, including agriculture and water management, the seasonality and timing of precipitation is just as important as the total amount. That is, changes in total precipitation can result in very different outcomes if the increased precipitation is delivered in extreme events or smaller more frequent events (Livneh *et al.*, 2024) and delivered as snow or rain (Lesk *et al.*, 2020). Thus, it is necessary to understand changes in the variability of precipitation in addition to long term averaged trends to produce relevant information about precipitation changes in response to global warming.

One of the largest drivers of global precipitation variability is the El Niño Southern Oscillation (ENSO) whose atmospheric component modulates the east-west Walker cell and the north-south Hadley circulation (Bjerknes, 1969; Ropelewski and Halpert, 1987; Mason and Goddard, 2001). During the positive ENSO phase (El Niño), the Walker circulation slows and shifts eastward.

This moves moisture convergence to the central Pacific, creating droughts in the Maritime Continent and Australia and increased precipitation in areas of South America (Mason and Goddard, 2001; Lenssen et al., 2020). Through teleconnections created by changes in atmospheric planetary waves originating from the tropics, regions beyond the tropics also experience precipitation anomalies associated with ENSO (Deser *et al.*, 2017; Yeh *et al.*, 2018; Lenssen *et al.*, 2020).

Because ENSO is a coupled phenomenon with multiple oceanic and atmospheric feedback processes interacting, understanding how ENSO responds to global warming remains challenging and highly uncertain. CMIP6 models generally predict a stronger ENSO in response to global warming (Fredriksen *et al.*, 2020; Cai *et al.*, 2022), yet large model differences and a comprehensive mechanism for driving these changes is lacking (Heede and Fedorov, 2023b). While the characteristics of ENSO and associated teleconnections itself may change in response to global warming (i.e. O'Brien and Deser, 2022; Maher *et al.*, 2023), changes in the pattern of warming across the tropical Pacific discussed above may also alter ENSO teleconnections and impacts. For example, more water vapor in the atmosphere is expected to create a more vigorous rainfall response to ENSO events (Yun *et al.*, 2021) as well as an eastward shift of the El Niño convection because of the higher absolute SST (Zhou *et al.*, 2014). These complex dynamical interactions make it difficult to determine if future changes to ENSO-related impacts assessed in fully coupled climate model projections are a result of an enhanced eastern Pacific warming, global warming, or changes to the ENSO amplitude itself (Bonfils *et al.*, 2015). Given the uncertainty in the eastern Pacific warming and ENSO amplitude, it is important to isolate and understand the impacts associated with each.

The purpose of this study is to specifically address both the role of enhanced eastern tropical Pacific warming and its interaction with ENSO in driving future changes in mean and extreme precipitation over the Americas. That is, addressing the model-observational tropical Pacific discrepancy in a mitigation and adaptation relevant context. In the modeling framework (Section 2), we conduct two sets of atmospheric general circulation model (AGCM) experiments using CESM-CAM6 that follow the SSP5-85 emission scenario from 2015-2100 with (EP) and without (noEP) prescribed enhanced eastern Pacific warming (Fig 1a, b). In addition, we prescribe an idealized ENSO cycle that is superimposed upon each of the background warming patterns (Fig 1c,d). We first consider large-scale changes in hydroclimates across the Americas and the difference between the EP and noEP experiments. We then illustrate how these changes manifest regionally and seasonally. Finally, we analyze how the interaction between ENSO and the mean state modulates ENSO related extreme events. We refer to previous literature for additional analysis and in-depth theory regarding the underlying dynamical teleconnection mechanisms, which drive tropically-induced changes in atmospheric moisture convergence (Seager and Vecchi, 2010; Seager, Naik and Vecchi, 2010; Bonfils *et al.*, 2015; Watterson, 2023)

2 Methods

2.1 Experimental design

Our experimental design consists of three A-GCM experiments with prescribed SST with 5 ensemble members apiece. The three experiments are: (a) a future with global warming and enhanced eastern Pacific warming (“EP”), (b) a future with global warming but without enhanced Pacific warming (“noEP”), (c) and a control simulation without time-evolving global warming ("Control"). SST anomalies associated with an idealized repeating ENSO cycle are superimposed in each experiment to investigate ENSO impacts as a function of background state changes. Our experiments are conducted with the atmosphere-land model components of Community Earth System Model version 2, namely Community Atmosphere Model version 6 (CAM6) coupled to Community Land Model version 5.0 (CLM5) (Danabasolu et al. 2020). Five ensemble members are generated for each experiment by altering the initial atmospheric temperatures by the order of 10^{-14} K (Kay *et al.*, 2015).

For the two warming experiments, the prescribed SSTs contain three components: (1) the observed seasonally-varying climatology, (2) an idealized repeating ENSO cycle, and (3) a linearly increasing 'global warming' SST pattern as described below and in Karnauskas *et al.* (2023). The data used for each component of the total prescribed SST is summarized in Table 1.

For the Control experiment, the prescribed SSTs are identical to those in the EP and noEP experiments except that the global warming trend component is omitted. For the EP and noEP experiments, atmospheric radiative forcing follows the SSP5-85 scenario and in the Control experiment, atmospheric radiative forcing conditions are fixed at year 2000 levels. As such, the Control experiment provides a baseline climatology from which effects due to both the Pacific warming pattern and global warming can be distinguished.

Component	*Dataset*	*Control*	*EP experiment*	*noEP experiment*
Linear warming trend	CESM1 Large ensemble, experiment no. 8 (sst_BRCP85C5CNBDRD_ens008_1x1_2006-2100_c141021) Kay et al. (2008)	Not included	Included	Included
Seasonal climatology	HadOIBl (Hurrell *et al.*, 2008) time period: 1870 to 2008	Included	Included	Included
ENSO idealized cycle	EOF calculated from ERA5 SST monthly mean (Hersbach *et al.*, 2020) from 1950 to 2021	Included	Included	Included
Tropical uniform smoothing	Spatial smoothing function applied to the linear warming trend dataset covering the area shown in Fig S1a	Not included	Not included	Included

Table 1. *Overview of the different components of the prescribed SST for each experiment including the datasets upon which the respective components are calculated.*

The linearly increasing global warming component is obtained by calculating the SST trend over the period 2015-2100 at each grid point from a fully coupled simulation of CESM1 under the RCP 8.5 emissions scenario. We use this pattern as representative of a typical CMIP SST warming pattern in response to global warming (Heede and Fedorov, 2021) where the eastern tropical Pacific warms more than other tropical ocean regions. We refer to the first experiment as **EP** (enhanced eastern tropical Pacific warming) in which the eastern equatorial warming pattern from the original experiment is retained (Fig. 1a). The second experiment is called **noEP** (no eastern tropical Pacific enhanced warming) in which the eastern equatorial Pacific warming signal is replaced by a uniform tropical warming pattern (Fig. 1b). The tropical warming pattern in the noEP experiment is computed in two steps. First, all grid cells in the two boxes (*170° E to 75° W, 10° S to 10° N* and *150° W to 60° W, 10° S to 30° S*, see Fig S1a) are replaced with the mean value of the corresponding box. Then, a smoothing kernel is applied at the edges of these two boxes to blend the modified SST values with the unmodified values and avoid sharp gradients (see Fig S1a for the extent of the smoothing kernel). All trends are linear in time so that the magnitudes of the patterns in Figs. 1a and 1b increase by a fixed amount at each time step over the years 2015-2100 (as illustrated in Fig. 1d). The two experiments differ in how much the tropical Pacific warms. However, they are virtually identical in their global mean climate sensitivity and hence the response in the hydrological cycle can be considered a direct response to the different patterns of warming rather than a response to differing rates of global warming. A consequence of the experimental design is that the zonal, meridional, and cross-ocean basin SST gradients between the three experiments evolve over time. The temporal evolution of select SST gradients for all three experiments is shown in Fig. S1.

While other studies using dynamically coupled ocean pacemaker experiments (Zhang *et al.*, 2019) are designed to obtain the most realistic climate response to a given regional SST anomaly pattern, our modeling framework is meant to isolate the terrestrial precipitation impacts strictly in response to tropical Pacific SST warming patterns. Therefore, we have designed our experiments so that only SST patterns in the tropical Pacific are altered but SSTs in the remaining ocean basins are unchanged (e.g., the so-called Tropical Ocean – Global Atmosphere TOGA set-up; see for example (Deser *et al.*, (2017)). Though this approach does not allow us to investigate the dynamical ocean response to the imposed SST anomaly, it does allow us to isolate the precipitation response directly arising from changes in the tropical Pacific and not from secondary effects of other ocean warming patterns formed in response to the imposed SST. Since only the eastern equatorial Pacific warming trend is replaced with tropically-uniform warming in the noEP experiment, we cannot address how interactions between projected warming trends in the Pacific and Atlantic and their interplay with ENSO may impact the hydroclimate in areas such as Central American and Caribbean (Herrera and Ault, 2017; Martinez *et al.*, 2022). Another caveat to consider is that we prescribe a linearized SST trend for simplicity. Yet in reality, decadal variability in the Pacific is likely to play an important role for the evolution of terrestrial hydroclimate (McCabe et al., 2004; Seager *et al.*, 2023). Overall, our experiments should be considered a sensitivity experiment answering the question, "Does the projected tropical Pacific warming pattern and its interaction with the ENSO cycle matter for terrestrial hydroclimate change?"

2.1.1 Idealized ENSO cycle

The prescribed idealized ENSO cycle is amplitude-symmetric and consists of one strong and one weak El Niño and La Niña per decade (Fig. 1d-e). Each prescribed idealized ENSO event follows a Gaussian function lasting exactly one year with a peak in December, similar to typical ENSO events in observations. Strong and weak idealized ENSO events correspond to maximum Niño3.4 anomalies of approximately ±2 and ±1 °C, respectively. The spatial pattern of ENSO is obtained from the leading global EOF of detrended SSTs during 1950-2020 from the ERSSTv5 instrumental reconstruction (Huang *et al.*, 2017, Fig. 1c). The seasonal SST climatology is based on the HadISST gridded reconstruction from 1982-2002 (Rayner *et al.*, 2003).

Our motivation for imposing this highly idealized ENSO cycle is to isolate strictly the effects of the superposition of ENSO-like interannual SST variations on a varying background state without considering changes to ENSO itself. If we attempted to mimic a more realistic ENSO cycle including, for example, weaker but longer lasting La Nina events, and eastern Pacific versus central Pacific events, it would be difficult to distinguish the effects on terrestrial hydroclimates arising from the ENSO background superposition from changes to the ENSO cycle itself without an excessively large number of ensemble members. As such, the goal of imposing an idealized ENSO cycle onto the EP and noEP experiments is to investigate how sensitive ENSO teleconnections are to a change in the background state, and as such should not be regarded as an attempt to be as realistic as possible.

2.2 Analysis methods

In order to highlight how tropical Pacific warming patterns affect the hydroclimate in the Americas, we apply the following analysis to the EP and noEP experiments:

1) For each grid cell and each ensemble member, we calculate the linear trends over the period 2015-2100 for precipitation (combined large-scale and convective), sea level pressure (SLP), and 250mb and 850mb winds for all months. We then mask out all grid cells where all 5 ensemble members do not agree on the sign of the trend. Next, we compute the difference between the ensemble averages of the EP and noEP experiments and conduct a Student's t-test for each grid cell and mask out grid cells where the differences are not statistically different at the 95% confidence interval using all 5 ensemble members.
2) To highlight the underlying large-scale dynamics driving changes in terrestrial precipitation, we next compute trends in upper-levels wind divergence (250 mb) following the same procedure as in 1) to illustrate spatial changes in tropical convection between the EP and noEP experiments. Next, we calculate integrated water vapor divergence to illustrate how changes in moisture divergence drive the observed changes in precipitation. The integrated moisture divergence $\nabla \cdot Q$ is calculated on monthly output following Trenberth and Guillemot (1998) and Xu *et al.* (2016):

$$\nabla \cdot Q = \nabla \cdot \frac{1}{g} \int_{Pmin}^{Ps} q\boldsymbol{v}\, dp$$

Where q is specific humidity, $\boldsymbol{v}$ is the horizontal velocity vector, g is the gravitational constant, P_s is 1000 mb, and P_{min} is 25 mb. We then evaluate the trends over time of moisture divergence $\nabla \cdot Q$ following same procedure as step 1).

3) We select 5 regions of interest in which we conduct a regional hydroclimate analysis. Three regions are selected visually from step 1) as regions that have a statistically significant precipitation trend between the EP and noEP experiments (Southern Mexico, Central America, Central Amazon and South-Eastern South America). An additional 2 regions, Western U.S. and Southern Chile, are selected to encompass regions that show significant differences in seasonal extreme precipitation between the two experiments (see section 4). We note that the Western U.S. box is chosen to include regions of the same sign in trend, El Niño-related precipitation response, and increase in El Niño-related extreme wet seasons. The regional extent of the 5 regions are as follows:
    a. Western U.S. (116° W to 124° W, 36° N to 44° N)
    b. Southern Mexico (95° W to 105° W, 15° N to 25° N)
    c. Central America (78° W to 88° W, 5° N to 21° N)
    d. Central Amazon (50° W to 70° W, 0° S to 10° S)
    e. South-Central South America (45° W to 60° W, 15° S to 30° S)
    f. Southern Chile (73° W to 78° W, 45° S to 55° S)

Precipitation trends are averaged spatially within these regions and a histogram is computed for 12-month smoothed timeseries across all 5 ensemble members of the EP, noEP and Control experiments to illustrate differences in the annual distributions between the EP and noEP experiments relative to the control experiment. Next, a 10-year smoothed time series is plotted to illustrate trends over time. Finally, trends are computed for each month of the year to illustrate the seasonal manifestation of the differences between the EP and noEP experiments and these are compared with the climatology from the Control experiment.

4) We quantify how the mean state of the tropical Pacific affects the distribution of end-of-century (2050-2100) boreal winter (DJFM) precipitation in the five regions of interest. As before, we determine anomalies in both the EP and noEP runs relative to a common climatology from the control simulation. The empirical distribution of regional rainfall is then calculated over El Niño, La Niña, and neutral DJFM periods from 2050-2100. We choose a 50-year period to improve estimates of the distribution as the results are qualitatively similar for shorter end-of-century periods.

5) We compare these end-of-century distributions to extreme quantiles from the control simulation to determine the role of the tropical Pacific mean state on seasonal extremes under global warming. Extreme dry and wet seasons are defined as the 2.5^{th} and 97.5^{th} percentiles of the DJFM regional precipitation in the control simulation calculated across all years and therefore all ENSO phases. The proportion of seasons with end-of-century seasonal extreme precipitation is thus calculated as the ratio of seasons exceeding this threshold over the total number of seasons.

3. Results

3.1 21st century precipitation trends in the Americas

The two experiments, noEP and EP, have broadly similar patterns of changes in precipitation and large-scale circulation (Fig. 2). In particular, the wetting along the west coast of Canada, Alaska, and central Argentina, and the drying trends in southern Mexico and Central America as well as the central Amazon region are robust responses to global warming that are relatively insensitive to the pattern of warming in the eastern tropical Pacific Ocean. However, there are some crucial differences between the two experiments (Fig. 2c) – namely a stronger drying trend along the Pacific coast of southern Mexico and Central America, and the Amazon region, in response to enhanced eastern Pacific warming. Meanwhile, in the EP experiment, the edges of this deep tropical drying trend shift equatorward resulting in the continental United States and subtropical South America are becoming on average when compared to noEP. In other words, the drying trends in the noEP experiment extend farther poleward. In the EP experiment, the drying trend is intensified in the deep tropics.

The Aleutian Low in the north Pacific intensifies in both warming experiments. However, it is stronger and shifts further eastward in EP (Fig. 2c). In the Southern Hemisphere midlatitudes, positive SLP anomalies are observed in both experiments, but in the EP experiment an intensification and eastward shift of the anticyclonic trend centered on the southern tip of South America is apparent (Fig 2b). Despite changes in extra-tropical SLP patterns, the long-term trends in terrestrial precipitation are generally not statistically different between the two experiments beyond latitudes of 30° N and 30° S.

To understand the dynamics driving exacerbated drying trends in the tropical American regions in the EP experiment, we examine the trends in moisture divergence and upper-level wind divergence (Figs. 3-4). The easterly trades in the tropical Pacific weaken in both experiments (Fig 3). This weakening is amplified in the EP experiment, resulting in a greater eastward shift of the Walker cell with anomalous deep convection (Fig. 4c) and moisture convergence (Fig 3c) in the central Pacific, and anomalous moisture divergence over the Maritime continent, Central America and the Amazon region, consistent with the canonical Bjerknes Feedback. Furthermore, an anomalous divergence of upper-level winds in the central Pacific and a convergence of upper-level winds in the Amazon region is observed, which suppresses convection and precipitation in this region (Fig 4c).

Not surprisingly, these differences in circulation and precipitation trends over the Americas between the EP and noEP experiments largely resemble the pattern of anomalies observed during El Niño events (Lenssen et al. 2020). However, we note that these changes are long-term trends averaged across all months and all phases of ENSO, enabling us to decompose this signal into the statistics of hydrological changes over all seasons. The following section describes the projected regional hydroclimate changes over the Americas and their dependence on the pattern of warming in the eastern Pacific in more detail.

3.2 Regional and seasonal precipitation trends across the Americas

Both south-central Mexico and Central America experience a shift in annual precipitation towards drier conditions (Fig. 5) which is exacerbated in the EP experiment. However, the seasonality of changes differs across these regions illustrating the interaction between the long-term Pacific warming trend and the mean climatology. In southern Mexico, the difference between EP and the noEP experiments is manifested primarily in October and November (Fig. 5c), while for Central America, the changes span the full calendar year (Fig. 5d). The central Amazon region is notable since the difference between the EP and noEP experiments is evident both as a mean shift towards drier conditions and a significant increase in extreme dry years in the EP experiment. For this region, the difference between the experiments is greatest in the months of February through August (Fig. 6f). In central-eastern South America, the difference between EP and noEP is opposite with a long-term drying trend emerging in the noEP experiment, but not in the EP experiment, reflecting the equatorward shift of drying trends (Fig. 6d-f) described in section 3.1.

Along the Western U.S. (Fig. 5a) and in southern Chile (Fig. 6g), differences between the EP and noEP experiment are not evident in the mean trend. However, in the Western U.S. region, the EP experiment results in more wet year extremes compared with the noEP experiment (Fig. 5a) whereas for southern Chile, the EP experiment results in more dry year extremes compared with the noEP experiment (Fig. 6i).

3.3 Changes in extreme precipitation stratified by ENSO phase

Next, we focus on the projected changes in extremely wet periods (defined as the frequency of events exceeding the 95th percentile of the Control simulation) in the two warming experiments during the DJFM and their dependence on ENSO phase. We investigate DJFM as the ENSO signal is strongest during this time. Fig. 7 shows that the frequency of wet extremes during

DJFM in Canada and Alaska occur in all 3 ENSO phases (Neutral, El Niño and La Nina). However, in the continental United States, wet extremes are more frequent during El Niño years than ENSO neutral years and nearly absent during La Nina years. In Central America and the Amazon region, dry extremes occur almost exclusively during El Niño years. Conversely, wet extremes in the Amazon region occur during La Nina years.

Fig. 8 shows the locations where there are statistically significant differences in extreme precipitation between the EP and noEP experiments for each ENSO phase. During ENSO neutral years, significant differences are limited to wet extremes over Canada, with fewer extreme wet winters in EP compared to noEP (Fig. 8a,b). The largest significant differences in extreme precipitation between EP and noEP occur mainly during El Niño years, with more extreme dry DJFM seasons in the Amazon and Central American regions and fewer in South-Central South America (Figs. 8e,f). The EP experiment also leads to more wet extremes along the Western U.S. and fewer wet extremes in Arctic Canada. During La Nina years, the EP experiment causes fewer wet extremes in the Central Amazon region relative to the noEP experiment.

To complement the spatial analysis, we examine future (2050-2100) changes in DJFM precipitation distributions during El Niño years *vs.* La Nina years in the EP and noEP experiments relative to the Control in the selected regions (Fig. 9). In the Western U.S., the most prominent difference between the two warming experiments occurs during El Niño years, with the EP experiment showing a shift toward more frequent wet extremes relative to the noEP experiment (compare solid orange vs. blue curves in Fig. 9a); La Nina years are relatively insensitive to the pattern of eastern tropical Pacific warming (comparing dashed orange vs. blue curves in Fig. 9a). In Central America, the EP experiment is drier than noEP in both La Nina and El Niño years (compare dashed and solid curves in Fig. 9b). As El Niño years are generally drier than La Niña years, the dry extremes (relative to Control) are also more prominent during El Niño compared to La Nina. In the central Amazon region, the difference between the EP and noEP experiments is amplified during El Niño years, which accounts for the most extreme dry years. In two cases, the noEP experiment shifts El Niño conditions more than the EP experiment. In southern Mexico, there is a shift towards wetter extremes during El Niño years for the noEP experiment (Fig. 9b), and for south-central South America, there is a shift towards drier conditions during El Niño (Fig. 9e.). Southern Chile, however, shows a shift towards drier conditions during El Niño years in both the EP and noEP experiments, but with more dry extremes in the EP experiment (Fig. 9f).

Overall, these results show that most differences of precipitation extremes between the EP and noEP experiment occur during El Niño events, illustrating how the background Pacific warming can modulate ENSO precipitation extremes without changes to ENSO amplitude itself. As illustrated in Fig. S1d, the absolute Pacific zonal SST gradient relative to Control is larger during El Niño years for both EP and noEP experiments (largest during EP experiments), likely driving the stronger extreme precipitation changes during El Niño years.

4 Discussion

This study has investigated how enhanced eastern equatorial Pacific SST warming projected by CMIP-class models (but not found in observations to date) significantly modulates future precipitation trends and variability across the Americas using a set of idealized AGCM experiments with CAM6. Similarly to El Niño events, an increase in deep convection and moisture convergence in the Pacific caused by enhanced eastern Pacific warming drives moisture divergence from the tropical American regions and an anomalous convergence of moisture in the Atlantic at 30°N and 30°S. The resultant difference in the spatial patterns of precipitation trends in the Americas between the experiments with and without enhanced eastern Pacific warming (EP *vs.* noEP) is a contraction and intensification of tropical drying trends: southern Mexico, Central America and the central Amazon region become drier on average in the EP experiment, while the continental US and the south-central part of South America become wetter. The differences in precipitation manifest heterogeneously seasonally and spatially. For instance, the difference between EP and noEP in Central America manifests as a year-round shift of the full distribution whereas differences in southern Mexico differences are largest in October and November and difference in the central Amazon region are largest in February through August.

In addition to driving long-term changes in mean precipitation, the EP and noEP warming experiments also induce extreme precipitation compared to the control experiment, especially during El Niño years. In the EP experiment, for example, dry extremes during El Niño are exacerbated greatly in Central America and the central Amazon region, but they are reduced in south-central South America (southern Brazil, Paraguay, Uruguay, and northern Argentina). This illustrates that the superposition of the ENSO cycle with different background warming patterns in the tropical Pacific can modulate the occurrence of extreme precipitation events over land, even in the absence of changes in ENSO amplitude.

These results are qualitatively similar to previous multi-model studies of forced hydroclimate trends (Seager and Vecchi, 2010; Watterson, 2023) and of forced changes to ENSO teleconnections (Beverley *et al.*, 2021; O'Brien and Deser, 2022), suggesting that the findings are not specific to our chosen AGCM. However, known biases in simulating convective and large-scale precipitation in AGCMs, and resultant biases in regional hydroclimates (i.e. Martinez *et al.*, 2024) should be kept in mind when evaluating these results.

The idealized ENSO cycle prescribed in our study was chosen to evaluate the effect of the mean state change on ENSO teleconnections in the absence of changes to ENSO variability itself. Thus by design, these experiments do not sample the full range of potential historical and projected ENSO events (Maher et al. 2023), including ENSO asymmetry and diversity (Capotondi *et al.*, 2015) and multi-year ENSO events (Okumura, DiNezio and Deser, 2017; Sanchez and Karnauskas, 2021). Thus, a complete range of potential future ENSO related impacts cannot be gauged from our experimental design. Yet, the simplicity of our design allows us to isolate how ENSO interacts with the mean state in future warming scenarios. This study provides a basis for future work evaluating extreme events associated with other changing ENSO characteristics, perhaps complemented by pacemaker experiments.

Our findings have important implications for adaptation and mitigation considerations as the presence or absence of enhanced eastern Pacific warming in the 21st century influences the severity and location of droughts and changes the distribution of extreme precipitation events in complex ways. By design, the EP and noEP experiments are constrained to be identical except for their tropical Pacific warming patterns; thus, we have used a "climate storyline" approach that explicitly considers potential uncertainties and systematic model biases in the response of the physical climate system to greenhouse gas forcing (Shepherd, 2019). We suggest this approach be used in regions beyond the Americas to better represent the full range of uncertainty in future tropical Pacific-driven changes in hydroclimate. The method can also be applied to understand the impacts of warming patterns in other ocean basins.

The sensitivity of the terrestrial hydroclimate to different ocean warming patterns found in this study illustrates the pressing importance of improving simulations of the coupled ocean-atmosphere response to anthropogenic forcing. Meanwhile, because the IPCC-class models do not currently capture the observed trends in global ocean warming patterns and hence may not accurately capture the future ocean warming patterns, expanding climate impact studies to consider possible future scenarios beyond those projected by IPCC models may offer important insights for climate adaption purposes.

Acknowledgements and funding sources

This research is funded by the Corporative Institute for Research in the Environmental Sciences (CIRES) Visiting Fellowship Program. We further acknowledge Adam Phillips at the National Center for Atmospheric Research for assistance with computational experiments as well as NCAR CISL grants UCUB0127, UCUB0131, UCUB0127 and UCUB0141. Publication of this article was funded by the University of Colorado Boulder Libraries Open Access Fund. The National Center for Atmospheric Research is sponsored by the National Science Foundation. We thank the two anonymous Reviewers for their constructive feedback on the original manuscript.

Data availability

All code used for analysis and visualization including a data subset to reproduce the figures is available here: https://doi.org/10.5281/zenodo.15831658

Model experiments are available at the National Center for Atmospheric Research.

4 References

Allen, M.R. and Ingram, W.J. (2002) 'Constraints on future changes in climate and the hydrologic cycle', *Nature*, 419(6903), pp. 224–232. Available at: https://doi.org/10.1038/nature01092.

Beverley, J.D. *et al.* (2021) 'Future changes to El Niño teleconnections over the north Pacific and North America', *Journal of Climate*, 34(15), pp. 6191–6205.

Bjerknes, J. (1969) 'Atmospheric teleconnections from the equatorial Pacific', *Monthly weather review*, 97(3), pp. 163–172.

Bloch-Johnson, J. *et al.* (2024) 'The Green's Function Model Intercomparison Project (GFMIP) Protocol', *Journal of Advances in Modeling Earth Systems*, 16(2), p. e2023MS003700. Available at: https://doi.org/10.1029/2023MS003700.

Bonfils, C.J. *et al.* (2015) 'Relative contributions of mean-state shifts and ENSO-driven variability to precipitation changes in a warming climate', *Journal of Climate*, 28(24), pp. 9997–10013.

Buchwald, A.G. *et al.* (2022) 'The Association Between Rainfall, Temperature, and Reported Drinking Water Source: A Multi-Country Analysis', *GeoHealth*, 6(11), p. e2022GH000605. Available at: https://doi.org/10.1029/2022GH000605.

Cai, W. *et al.* (2022) 'Increased ENSO sea surface temperature variability under four IPCC emission scenarios', *Nature Climate Change*, 12(3), pp. 228–231. Available at: https://doi.org/10.1038/s41558-022-01282-z.

Capotondi, A. *et al.* (2015) 'Understanding ENSO Diversity', *Bulletin of the American Meteorological Society*, 96(6), pp. 921–938. Available at: https://doi.org/10.1175/BAMS-D-13-00117.1.

Chou, C. and Neelin, J.D. (2004) 'Mechanisms of Global Warming Impacts on Regional Tropical Precipitation', *Journal of Climate*, 17(13), pp. 2688–2701. Available at: https://doi.org/10.1175/1520-0442(2004)017<2688:MOGWIO>2.0.CO;2.

Clement, A.C. *et al.* (1996) 'An ocean dynamical thermostat', *Journal of Climate*, 9(9), pp. 2190–2196.

Crochemore, L., Ramos, M.-H. and Pappenberger, F. (2016) 'Bias correcting precipitation forecasts to improve the skill of seasonal streamflow forecasts', *Hydrology and Earth System Sciences*, 20(9), pp. 3601–3618. Available at: https://doi.org/10.5194/hess-20-3601-2016.

Deser, C. *et al.* (2017) 'The Northern Hemisphere Extratropical Atmospheric Circulation Response to ENSO: How Well Do We Know It and How Do We Evaluate Models Accordingly?', *Journal of Climate*, 30(13), pp. 5059–5082. Available at: https://doi.org/10.1175/JCLI-D-16-0844.1.

Devereux, S. (2007) 'The impact of droughts and floods on food security and policy options to alleviate negative effects', *Agricultural Economics*, 37(s1), pp. 47–58. Available at: https://doi.org/10.1111/j.1574-0862.2007.00234.x.

DiNezio, P., Clement, A. and Vecchi, G. (2010) 'Reconciling Differing Views of Tropical Pacific Climate Change', *Eos, Transactions American Geophysical Union*, 91(16), pp. 141–142. Available at: https://doi.org/10.1029/2010EO160001.

Dong, B. and Lu, R. (2013) 'Interdecadal enhancement of the Walker circulation over the tropical Pacific in the late 1990s', *Advances in Atmospheric Sciences*, 30(2), pp. 247–262.

Dong, Y. *et al.* (2019) 'Attributing Historical and Future Evolution of Radiative Feedbacks to Regional Warming Patterns using a Green's Function Approach: The Preeminence of the Western Pacific'. Available at: https://doi.org/10.1175/JCLI-D-18-0843.1.

Dong, Y. *et al.* (2022) 'Two-way teleconnections between the Southern Ocean and the tropical Pacific via a dynamic feedback', *Journal of Climate*, 35(19), pp. 2667–2682.

Fosu, B., He, J. and Liguori, G. (2020) 'Equatorial Pacific Warming Attenuated by SST Warming Patterns in the Tropical Atlantic and Indian Oceans', *Geophysical Research Letters*, 47(18), p. e2020GL088231. Available at: https://doi.org/10.1029/2020GL088231.

Fredriksen, H.-B. *et al.* (2020) 'How Does El Niño–Southern Oscillation Change Under Global Warming—A First Look at CMIP6', *Geophysical Research Letters*, 47(22), p. e2020GL090640. Available at: https://doi.org/10.1029/2020GL090640.

Greve, P. *et al.* (2014) 'Global assessment of trends in wetting and drying over land', *Nature Geoscience*, 7(10), pp. 716–721. Available at: https://doi.org/10.1038/ngeo2247.

Gulev, S.K. *et al.* (2021) 'Chapter 2: Changing State of the Climate System', in V. Masson-Delmotte et al. (eds) *Climate Change 2021: The Physical Science Basis. Contribution of Working Group I to the Sixth Assessment Report of the Intergovernmental Panel on Climate Change*. Cambridge, United Kingdom and New York, NY, USA: Cambridge University Press, Cambridge.

Harp, R.D. *et al.* (2021) 'Interannual Climate Variability and Malaria in Mozambique', *GeoHealth*, 5(2), p. e2020GH000322. Available at: https://doi.org/10.1029/2020GH000322.

He, C. and Li, T. (2019) 'Does global warming amplify interannual climate variability?', *Climate Dynamics*, 52(5), pp. 2667–2684. Available at: https://doi.org/10.1007/s00382-018-4286-0.

Heede, U. and Fedorov, A. (2021) 'Eastern equatorial Pacific warming delayed by aerosols and thermostat response to CO2'.

Heede, U.K. and Fedorov, A.V. (2023a) 'Colder Eastern Equatorial Pacific and Stronger Walker Circulation in the Early 21st Century: Separating the Forced Response to Global Warming From Natural Variability', *Geophysical Research Letters*, 50(3), p. e2022GL101020. Available at: https://doi.org/10.1029/2022GL101020.

Heede, U.K. and Fedorov, A.V. (2023b) 'Towards understanding the robust strengthening of ENSO and more frequent extreme El Niño events in CMIP6 global warming simulations', *Climate Dynamics*, 61(5), pp. 3047–3060. Available at: https://doi.org/10.1007/s00382-023-06856-x.

Heede, U.K., Fedorov, A.V. and Burls, N.J. (2020) 'Timescales and mechanisms for the Tropical Pacific response to global warming: a tug of war between the Ocean Thermostat and weaker Walker', *Journal of Climate* [Preprint]. Available at: https://doi.org/10.1175/JCLI-D-19-0690.1.

Held, I.M. and Soden, B.J. (2006) 'Robust responses of the hydrological cycle to global warming', *Journal of climate*, 19(21), pp. 5686–5699.

Herrera, D. and Ault, T. (2017) 'Insights from a New High-Resolution Drought Atlas for the Caribbean Spanning 1950–2016'. Available at: https://doi.org/10.1175/JCLI-D-16-0838.1.

Hersbach, H. *et al.* (2020) 'The ERA5 global reanalysis', *Quarterly Journal of the Royal Meteorological Society*, 146(730), pp. 1999–2049. Available at: https://doi.org/10.1002/qj.3803.

Hong, Y., Adler, R. and Huffman, G. (2007) 'Use of satellite remote sensing data in the mapping of global landslide susceptibility', *Natural Hazards*, 43(2), pp. 245–256. Available at: https://doi.org/10.1007/s11069-006-9104-z.

Hu, S. and Fedorov, A.V. (2019) 'Indian Ocean warming can strengthen the Atlantic meridional overturning circulation', *Nature Climate Change*, 9(10), pp. 747–751. Available at: https://doi.org/10.1038/s41558-019-0566-x.

Huang, B. *et al.* (2017) 'NOAA extended reconstructed sea surface temperature (ERSST), version 5', *NOAA National Centers for Environmental Information*, 30, pp. 8179–8205.

Hurrell, J.W. *et al.* (2008) 'A New Sea Surface Temperature and Sea Ice Boundary Dataset for the Community Atmosphere Model'. Available at: https://doi.org/10.1175/2008JCLI2292.1.

Hwang, Y.-T. *et al.* (2024) ‘Contribution of anthropogenic aerosols to persistent La Niña-like conditions in the early 21st century’, *Proceedings of the National Academy of Sciences*, 121(5), p. e2315124121. Available at: https://doi.org/10.1073/pnas.2315124121.

Jiang, F., Seager, R. and Cane, M.A. (2024) ‘Historical subsurface cooling in the tropical Pacific and its dynamics’, *Journal of Climate*, 37(22), pp. 5925–5938.

Kang, S.M. *et al.* (2023) ‘Disentangling the mechanisms of equatorial Pacific climate change’, *Science Advances*, 9(19), p. eadf5059. Available at: https://doi.org/10.1126/sciadv.adf5059.

Karnauskas, K.B., Heede, U.K. and Zhang, L. (2023) ‘The Impact of Eastern Pacific Warming on Future North Atlantic Tropical Cyclogenesis’, *Geophysical Research Letters*, 50(17), p. e2023GL105551. Available at: https://doi.org/10.1029/2023GL105551.

Kay, J.E. *et al.* (2015) ‘The Community Earth System Model (CESM) large ensemble project: A community resource for studying climate change in the presence of internal climate variability’, *Bulletin of the American Meteorological Society*, 96(8), pp. 1333–1349.

Keil, P. *et al.* (2020) ‘Multiple drivers of the North Atlantic warming hole’, *Nature Climate Change*, 10(7), pp. 667–671. Available at: https://doi.org/10.1038/s41558-020-0819-8.

Kosaka, Y. and Xie, S.-P. (2013) ‘Recent global-warming hiatus tied to equatorial Pacific surface cooling’, *Nature*, 501(7467), pp. 403–407. Available at: https://doi.org/10.1038/nature12534.

Kotz, M., Levermann, A. and Wenz, L. (2022) ‘The effect of rainfall changes on economic production’, *Nature*, 601(7892), pp. 223–227. Available at: https://doi.org/10.1038/s41586-021-04283-8.

Lenssen, N.J.L. *et al.* (2019) ‘Improvements in the GISTEMP Uncertainty Model’, *Journal of Geophysical Research: Atmospheres*, 124(12), pp. 6307–6326. Available at: https://doi.org/10.1029/2018JD029522.

Lenssen, N.J.L., Goddard, L. and Mason, S. (2020) ‘Seasonal Forecast Skill of ENSO Teleconnection Maps’, *Weather and Forecasting*, 35(6), pp. 2387–2406. Available at: https://doi.org/10.1175/WAF-D-19-0235.1.

Lesk, C., Coffel, E. and Horton, R. (2020) ‘Net benefits to US soy and maize yields from intensifying hourly rainfall’, *Nature Climate Change*, 10(9), pp. 819–822. Available at: https://doi.org/10.1038/s41558-020-0830-0.

Livneh, B. *et al.* (2024) ‘Can precipitation intermittency predict flooding?’, *Science of The Total Environment*, 945, p. 173824. Available at: https://doi.org/10.1016/j.scitotenv.2024.173824.

Maher, N. *et al.* (2023) ‘The future of the El Niño–Southern Oscillation: using large ensembles to illuminate time-varying responses and inter-model differences’, *Earth System Dynamics*, 14(2), pp. 413–431. Available at: https://doi.org/10.5194/esd-14-413-2023.

Manabe, S. and Wetherald, R.T. (1975) ‘The Effects of Doubling the CO2 Concentration on the climate of a General Circulation Model’, *Journal of the Atmospheric Sciences*, 32(1), pp. 3–15. Available at: https://doi.org/10.1175/1520-0469(1975)032<0003:TEODTC>2.0.CO;2.

Martinez, C. *et al.* (2022) ‘Seasonal prediction of the Caribbean rainfall cycle’, *Climate Services*, 27, p. 100309. Available at: https://doi.org/10.1016/j.cliser.2022.100309.

Martinez, C.J. *et al.* (2024) ‘An evaluation of the seasonal Caribbean hydroclimate in low and high-resolution CESM and other CMIP6 models’, *Climate Dynamics*, 63(1), p. 33. Available at: https://doi.org/10.1007/s00382-024-07516-4.

Mason, S.J. and Goddard, L. (2001) ‘Probabilistic Precipitation Anomalies Associated with EN SO’, *Bulletin of the American Meteorological Society*, 82(4), pp. 619–638. Available at: https://doi.org/10.1175/1520-0477(2001)082<0619:PPAAWE>2.3.CO;2.

McCabe, G.J., Palecki, M.A. and Betancourt, J.L. (2004) ‘Pacific and Atlantic Ocean influences on multidecadal drought frequency in the United States’, *Proceedings of the National Academy of Sciences*, 101(12), pp. 4136–4141. Available at: https://doi.org/10.1073/pnas.0306738101.

Meehl, G.A., Wheeler, M. and Washington, W.M. (1994) ‘Low-frequency variability and CO2 transient climate change. Part 3. Intermonthly and interannual variability’, *Climate Dynamics*, 10(6), pp. 277–303. Available at: https://doi.org/10.1007/BF00228028.

Morice, C.P. *et al.* (2021) ‘An Updated Assessment of Near-Surface Temperature Change From 1850: The HadCRUT5 Data Set’, *Journal of Geophysical Research: Atmospheres*, 126(3), p. e2019JD032361. Available at: https://doi.org/10.1029/2019JD032361.

Nadim, F. *et al.* (2006) ‘Global landslide and avalanche hotspots’, *Landslides*, 3(2), pp. 159–173. Available at: https://doi.org/10.1007/s10346-006-0036-1.

O’Brien, J.P. and Deser, C. (2022) ‘Quantifying and Understanding Forced Changes to Unforced Modes of Atmospheric Circulation Variability over the North Pacific in a Coupled Model Large Ensemble’, *Journal of Climate*, 36(1), pp. 19–37. Available at: https://doi.org/10.1175/JCLI-D-22-0101.1.

Okumura, Y.M., DiNezio, P. and Deser, C. (2017) ‘Evolving Impacts of Multiyear La Niña Events on Atmospheric Circulation and U.S. Drought’, *Geophysical Research Letters*, 44(22), p. 11,614-11,623. Available at: https://doi.org/10.1002/2017GL075034.

Pendergrass, A.G. *et al.* (2017) ‘Precipitation variability increases in a warmer climate’, *Scientific Reports*, 7(1), p. 17966. Available at: https://doi.org/10.1038/s41598-017-17966-y.

Pfahl, S., O’Gorman, P.A. and Fischer, E.M. (2017) ‘Understanding the regional pattern of projected future changes in extreme precipitation’, *Nature Climate Change*, 7(6), pp. 423–427. Available at: https://doi.org/10.1038/nclimate3287.

Rayner, N.A. *et al.* (2003) 'Global analyses of sea surface temperature, sea ice, and night marine air temperature since the late nineteenth century', *Journal of Geophysical Research: Atmospheres*, 108(D14). Available at: https://doi.org/10.1029/2002JD002670.

Ropelewski, C.F. and Halpert, M.S. (1987) 'Global and Regional Scale Precipitation Patterns Associated with the El Niño/Southern Oscillation', *Monthly Weather Review*, 115(8), pp. 1606–1626. Available at: https://doi.org/10.1175/1520-0493(1987)115<1606:GARSPP>2.0.CO;2.

Sanchez, S.C. and Karnauskas, K.B. (2021) 'Diversity in the Persistence of El Niño Events Over the Last Millennium', *Geophysical Research Letters*, 48(18), p. e2021GL093698. Available at: https://doi.org/10.1029/2021GL093698.

Schwarzwald, K. *et al.* (2021) 'Changes in Future Precipitation Mean and Variability across Scales', *Journal of Climate*, 34(7), pp. 2741–2758. Available at: https://doi.org/10.1175/JCLI-D-20-0001.1.

Seager, R. *et al.* (2019) 'Strengthening tropical Pacific zonal sea surface temperature gradient consistent with rising greenhouse gases', *Nature Climate Change*, 9(7), pp. 517–522.

Seager, R. *et al.* (2023) 'Ocean-forcing of cool season precipitation drives ongoing and future decadal drought in southwestern North America', *npj Climate and Atmospheric Science*, 6(1), pp. 1–12. Available at: https://doi.org/10.1038/s41612-023-00461-9.

Seager, R., Henderson, N. and Cane, M. (2022) 'Persistent discrepancies between observed and modeled trends in the tropical Pacific Ocean', *Journal of Climate*, 1(aop), pp. 1–41. Available at: https://doi.org/10.1175/JCLI-D-21-0648.1.

Seager, R., Naik, N. and Vecchi, G.A. (2010) 'Thermodynamic and dynamic mechanisms for large-scale changes in the hydrological cycle in response to global warming', *Journal of climate*, 23(17), pp. 4651–4668.

Seager, R. and Vecchi, G.A. (2010) 'Greenhouse warming and the 21st century hydroclimate of southwestern North America', *Proceedings of the National Academy of Sciences*, 107(50), pp. 21277–21282. Available at: https://doi.org/10.1073/pnas.0910856107.

Shepherd, T.G. (2019) 'Storyline approach to the construction of regional climate change information', *Proceedings of the Royal Society A: Mathematical, Physical and Engineering Sciences*, 475(2225), p. 20190013. Available at: https://doi.org/10.1098/rspa.2019.0013.

Sun, D.-Z. and Liu, Z. (1996) 'Dynamic ocean-atmosphere coupling: A thermostat for the tropics', *Science*, 272(5265), pp. 1148–1150.

Trenberth, K.E. and Guillemot, C.J. (1998) 'Evaluation of the atmospheric moisture and hydrological cycle in the NCEP/NCAR reanalyses', *Climate Dynamics*, 14(3), pp. 213–231. Available at: https://doi.org/10.1007/s003820050219.

Vecchi, G.A. and Soden, B.J. (2007) 'Global warming and the weakening of the tropical circulation', *Journal of Climate*, 20(17), pp. 4316–4340.

Vicente-Serrano, S.M. *et al.* (2013) 'Response of vegetation to drought time-scales across global land biomes', *Proceedings of the National Academy of Sciences*, 110(1), pp. 52–57. Available at: https://doi.org/10.1073/pnas.1207068110.

Walker, G.T. (1925) 'CORRELATION IN SEASONAL VARIATIONS OF WEATHER—A FURTHER STUDY OF WORLD WEATHER', *Monthly Weather Review*, 53(6), pp. 252–254. Available at: https://doi.org/10.1175/1520-0493(1925)53<252:CISVOW>2.0.CO;2.

Watanabe, M. *et al.* (2024) 'Possible shift in controls of the tropical Pacific surface warming pattern', *Nature*, 630(8016), pp. 315–324. Available at: https://doi.org/10.1038/s41586-024-07452-7.

Watanabe, T. *et al.* (2018) 'Management of Climatic Extremes with Focus on Floods and Droughts in Agriculture', *Irrigation and Drainage*, 67(1), pp. 29–42. Available at: https://doi.org/10.1002/ird.2204.

Watterson, I.G. (2023) 'Atmospheric Moisture Transport Associated with Precipitation in Present and Simulated Future Climates', *Journal of Climate*, 36(18), pp. 6409–6425.

Wetherald, R.T. and Manabe, S. (2002) 'Simulation of hydrologic changes associated with global warming', *Journal of Geophysical Research: Atmospheres*, 107(D19), p. ACL 7-1-ACL 7-15. Available at: https://doi.org/10.1029/2001JD001195.

Wills, R.C.J. *et al.* (2022) 'Systematic Climate Model Biases in the Large-Scale Patterns of Recent Sea-Surface Temperature and Sea-Level Pressure Change', *Geophysical Research Letters*, 49(17), p. e2022GL100011. Available at: https://doi.org/10.1029/2022GL100011.

Wu, M. *et al.* (2021) 'A very likely weakening of Pacific Walker Circulation in constrained near-future projections', *Nature Communications*, 12(1), p. 6502. Available at: https://doi.org/10.1038/s41467-021-26693-y.

Xie, S.-P. *et al.* (2010) 'Global warming pattern formation: Sea surface temperature and rainfall', *Journal of Climate*, 23(4), pp. 966–986.

Xu, G. *et al.* (2016) 'Different atmospheric moisture divergence responses to extreme and moderate El Niños', *Climate Dynamics*, 47(1), pp. 393–410. Available at: https://doi.org/10.1007/s00382-015-2844-2.

Yeh, S.-W. *et al.* (2018) 'ENSO Atmospheric Teleconnections and Their Response to Greenhouse Gas Forcing', *Reviews of Geophysics*, 56(1), pp. 185–206. Available at: https://doi.org/10.1002/2017RG000568.

Ying, J. *et al.* (2022) 'Emergence of climate change in the tropical Pacific', *Nature Climate Change*, pp. 1–9. Available at: https://doi.org/10.1038/s41558-022-01301-z.

Yun, K.-S. *et al.* (2021) 'Increasing ENSO–rainfall variability due to changes in future tropical temperature–rainfall relationship', *Communications Earth & Environment*, 2(1), pp. 1–7. Available at: https://doi.org/10.1038/s43247-021-00108-8.

Zhang, L. *et al.* (2019) ‘Indian Ocean Warming Trend Reduces Pacific Warming Response to Anthropogenic Greenhouse Gases: An Interbasin Thermostat Mechanism’, *Geophysical Research Letters*, 46(19), pp. 10882–10890.

Zhou, Z.-Q. *et al.* (2014) ‘Global Warming–Induced Changes in El Niño Teleconnections over the North Pacific and North America’, *Journal of Climate*, 27(24), pp. 9050–9064. Available at: https://doi.org/10.1175/JCLI-D-14-00254.1.

5 Figures

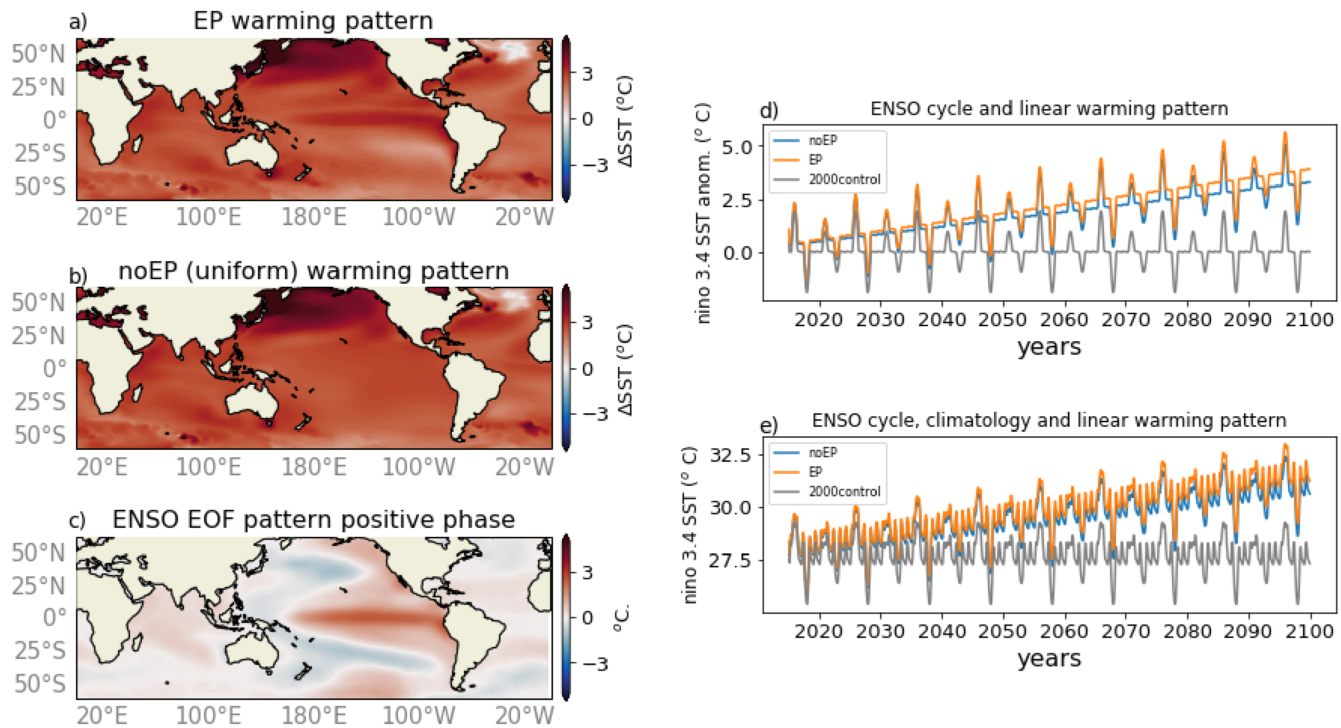

Figure 1. EP and noEP warming patterns, and idealized ENSO cycle. *a) and b) SST anomalies averaged from 2080 to 2100 in the noEP and EP experiments, respectively. c) maximum positive phase of the EOF pattern applied in the idealized ENSO cycle. d) Niño3.4 SST timeseries in the EP (orange), noEP (blue) and 2000control (gray) experiments after removing the climatological seasonal cycle from the 2000control. e) same as d) but including the climatology*

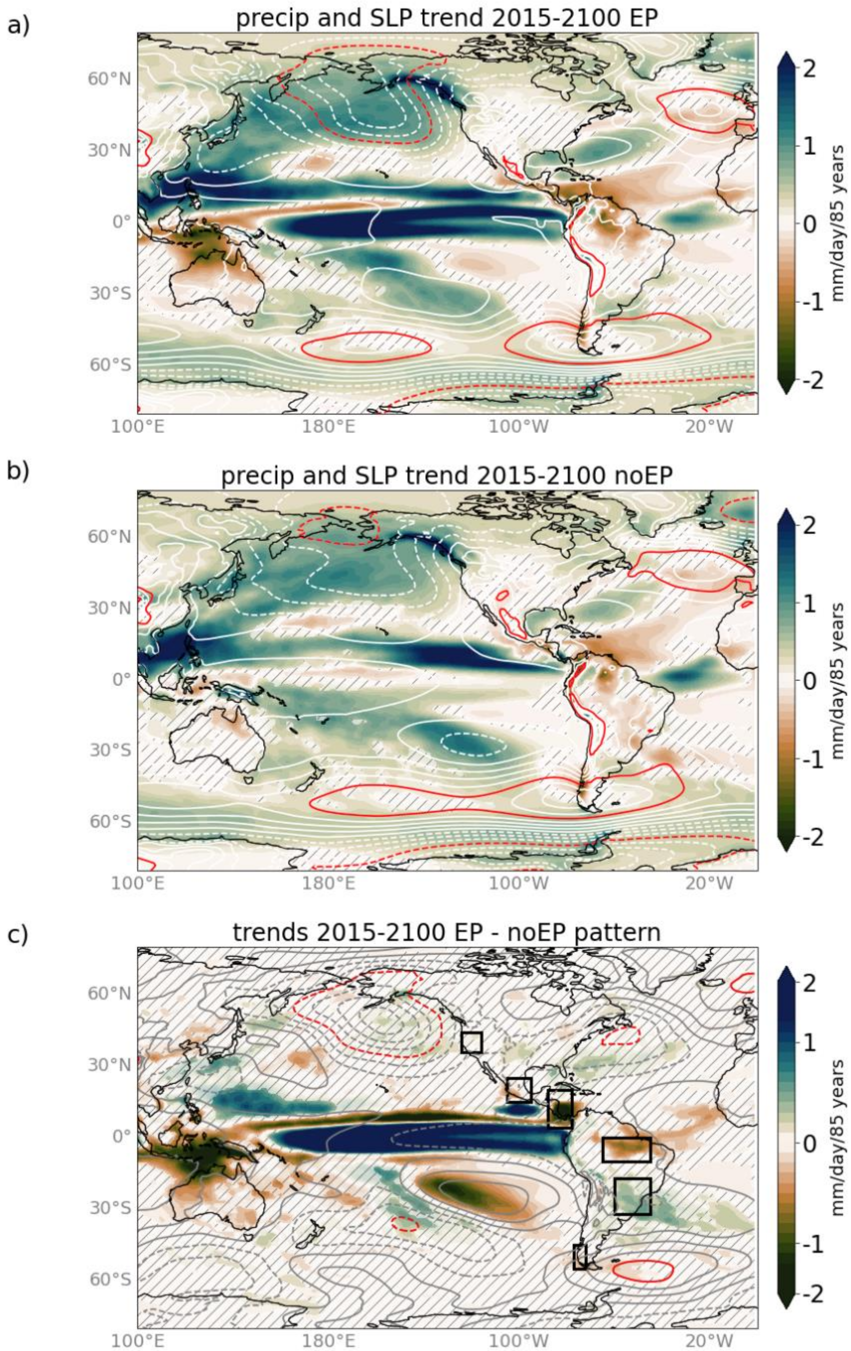

Figure 2. Precipitation (color shading) and sea-level pressure (SLP; contours) trends from 2015-2100 based on all months for the *a) EP experiment, b) noEP experiment and c) their difference (EP – noEP). Hatching in a) and b) indicates regions where not all ensemble members agree on the sign of the precipitation trend; hatching in c) indicates regions where the difference between the precipitation trends in the EP and noEP experiments is not statistically significant at the 95% confidence interval based on a Student's t-test. The orange boxes indicate areas used for regional plots. In a) and b), the SLP contour interval is 0.50 hPa (negative values dashed, positive values solid) and the 2.00 hPa contours are highlighted in red. In c), the SLP contour interval is 0.25 hPa and the 0.75 hPa contours are highlighted in red.*

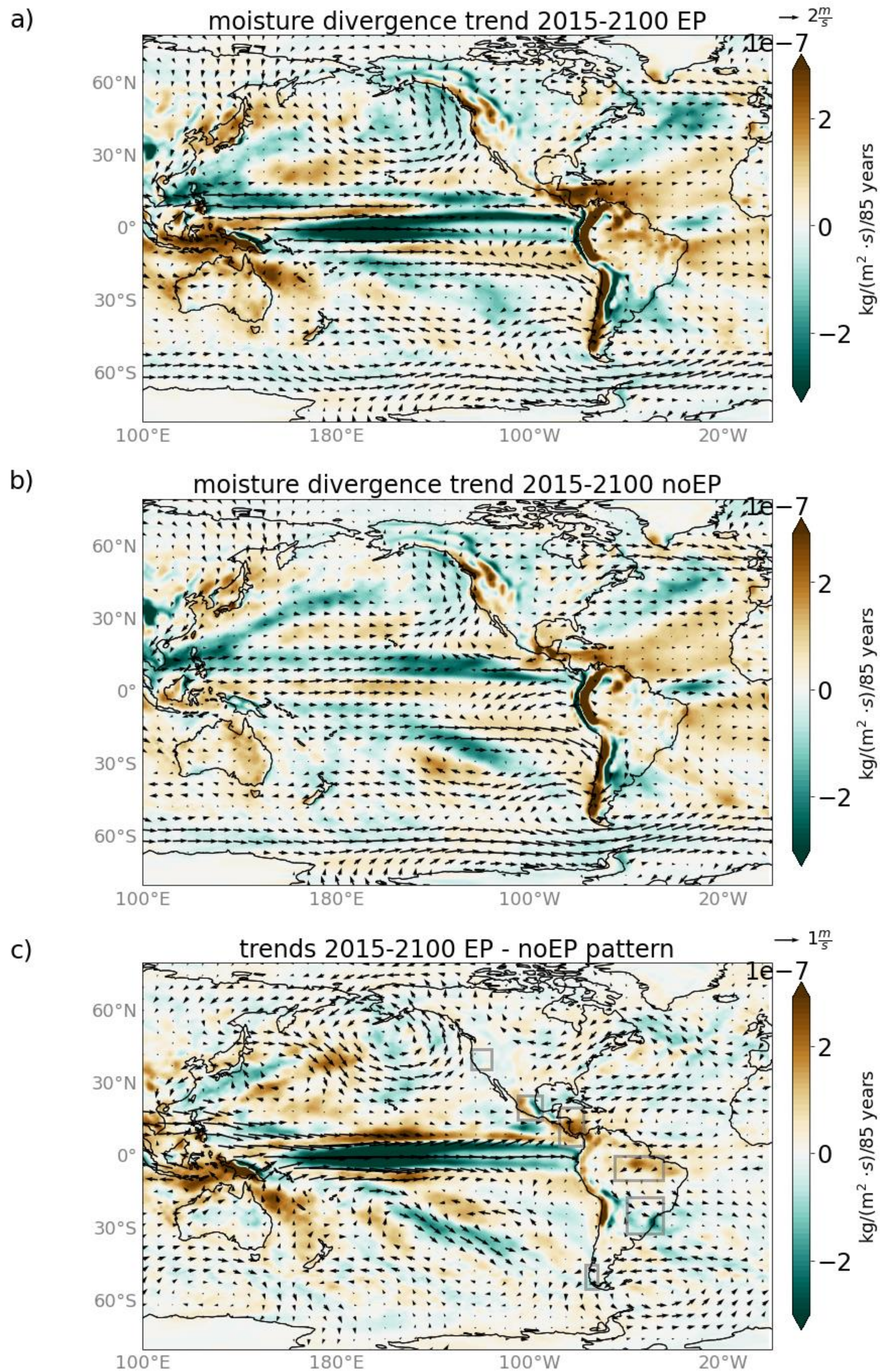

Figure 3. As in Fig. 2 but for column-integrated moisture divergence (color shading) and 850mb winds (vectors). *In a) and b), the reference vector is 2 m/s and in c), the reference vector is 1 m/s.*

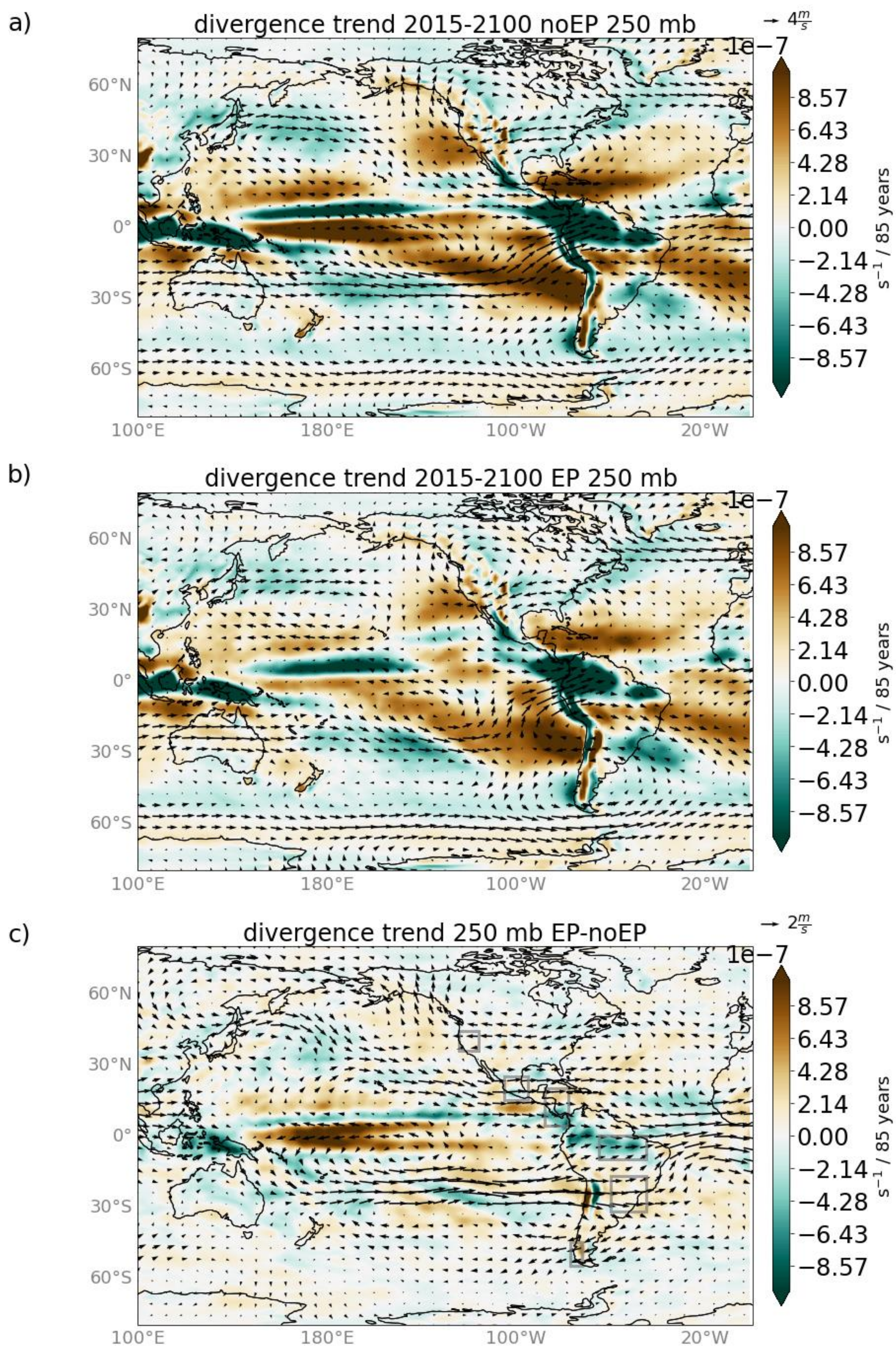

Figure 4. As in Fig. 2 but for upper level (250 mb) wind divergence (color shading) and 250mb winds (vectors) *In a) and b), the reference vector is 4 m/s and in c) the reference vector is 2 m/s.*

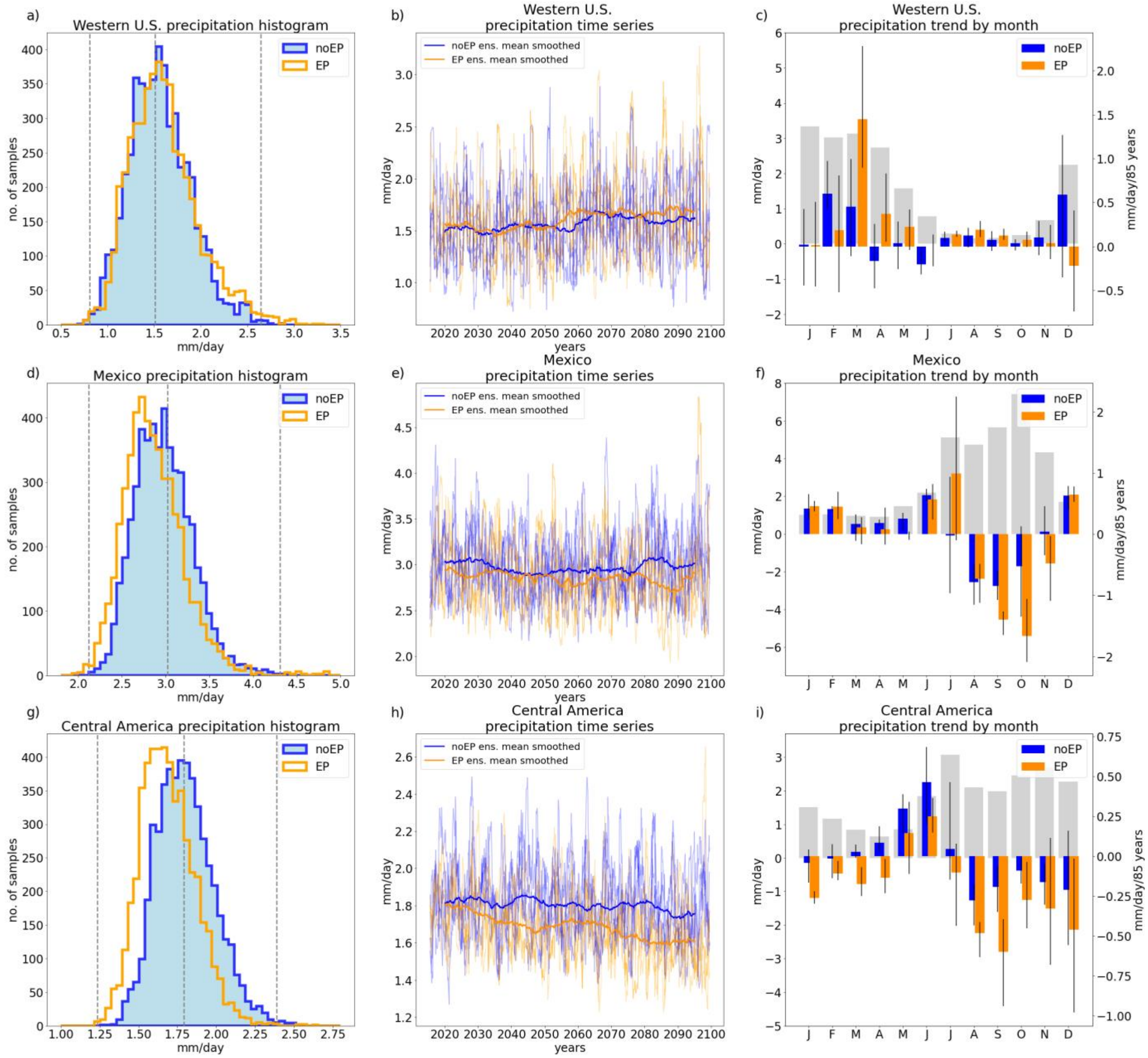

***Figure 5. Regional overview of precipitation responses in the EP and noEP experiments for the Western U.S., Mexico and Central America (regions outlined in Fig. 1c)**. Left: histogram of monthly precipitation from 2015 to 2100 (mm/day) after applying a 12-month running mean to the data. The vertical grey dashed lines represent the minimum, median and maximum values of the 2000control simulation across the 5 ensembles. Middle: monthly precipitation timeseries from the individual ensemble members (thin curves) and the ensemble mean after applying a 10-year running mean (thick curves). Right: precipitation trend from 2015 to 2100 for each month, with grey bars representing the climatology from the 2000control experiment. In all panels, the noEP experiment is shown in blue and the EP experiment is shown in orange.*

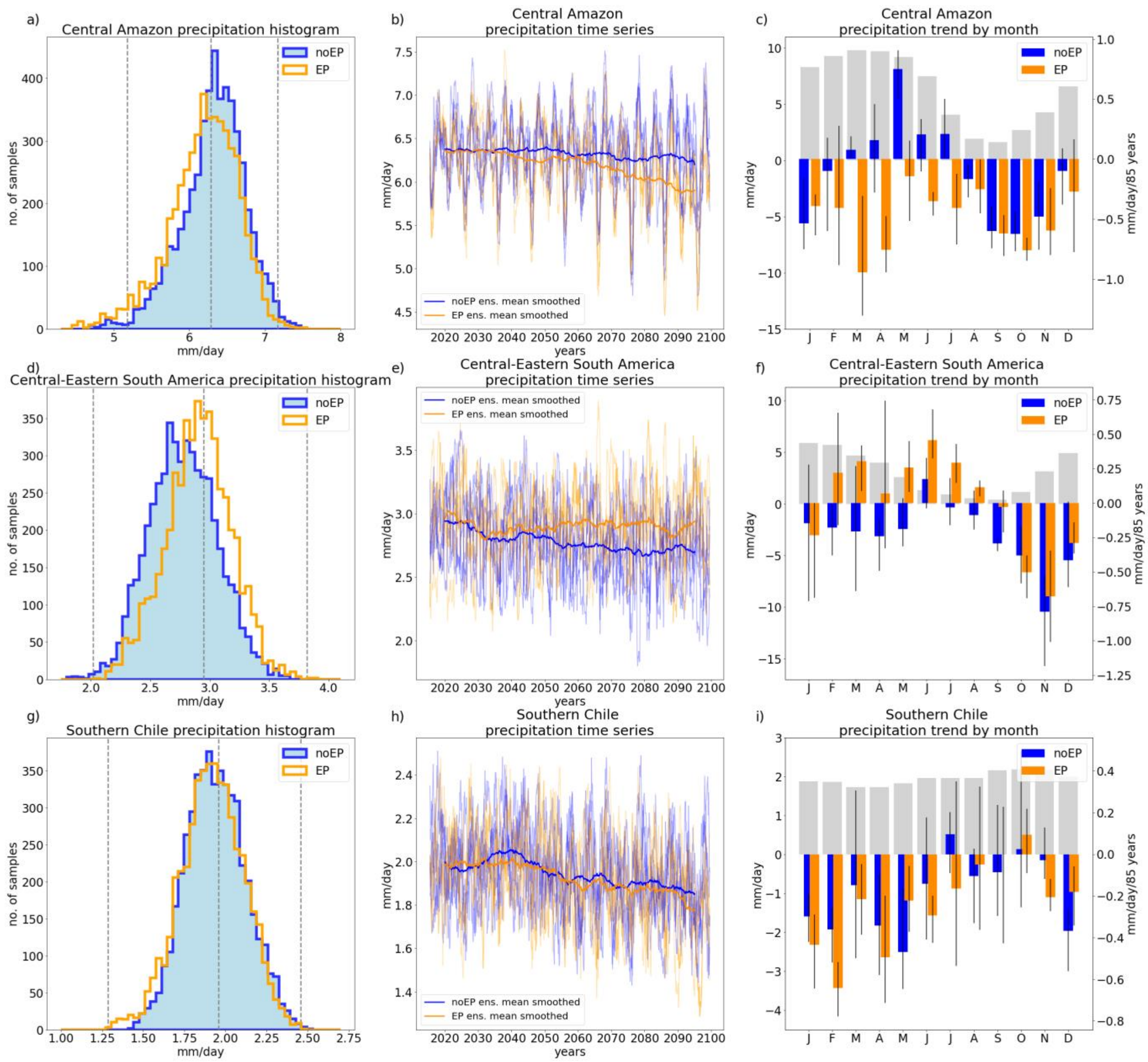

***Figure 6. As in Fig. 5 but for the Central Amazon region, Central-Eastern South America and Southern Chile*.**

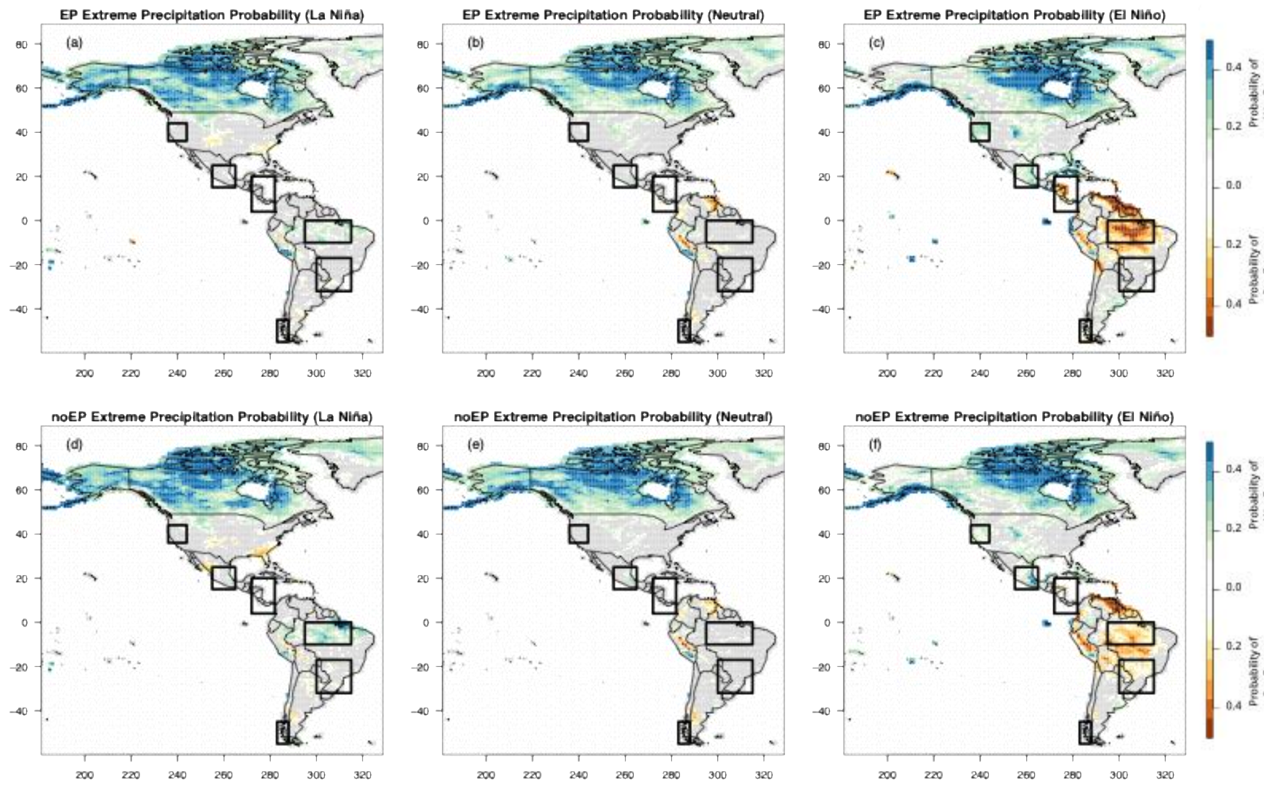

Figure 7. Frequency of 2050-2100 extreme DJFM precipitation in EP and noEP experiments during three phases of ENSO. *The empirical probability of extreme wet and dry DJFM in 2050-2100 during La Niña (left column), Neutral (middle column) and El Niño (right column) for the EP (first row) and the noEP (second row) experiments. Wet extremes are defined as a DJFM below the 2.5th percentile of the 2000control and dry extremes are defined as DJFM above the 97.5th percentile of the 2000control. Regions that do not have probabilities of wet or dry DJFM extremes statistically different from the 2000control are shaded in grey.*

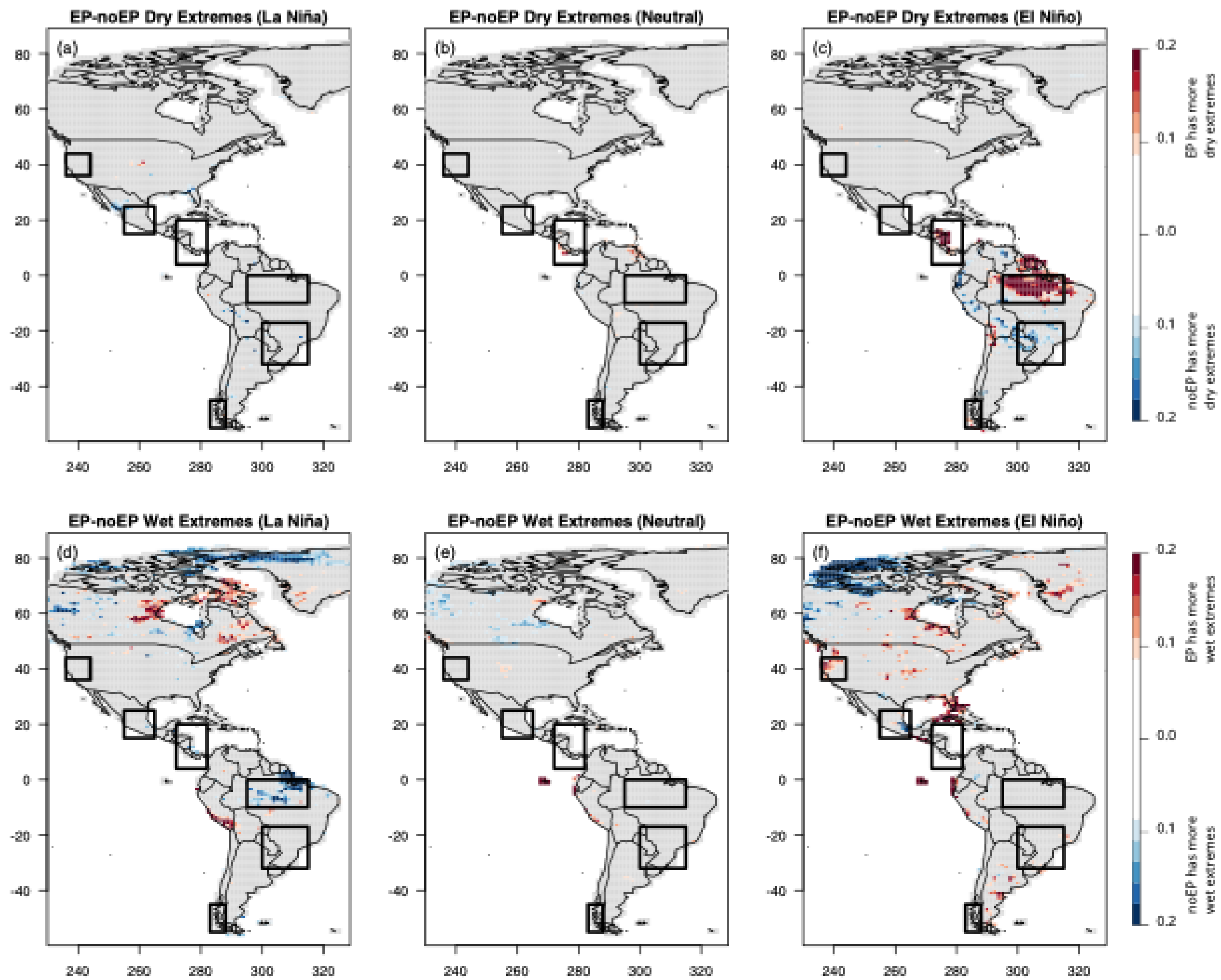

Figure 8. The difference in the probability of dry and wet extreme DJFM between the EP and noEP experiments (2050-2100). *The difference in the empirical probability of dry extremes (top row) and wet extremes (bottom row) as calculated as the difference of EP-noEP as shown in Figure 7. Red colors indicate an extreme DJFM is more likely under the EP experiment. The differences are shown for La Niña years (left column), for neutral years (middle column), and for El Niño years (right column). Areas that do not show a statistically significant difference in the rate of precipitation extremes between the EP and noEP experiments are shaded in grey.*

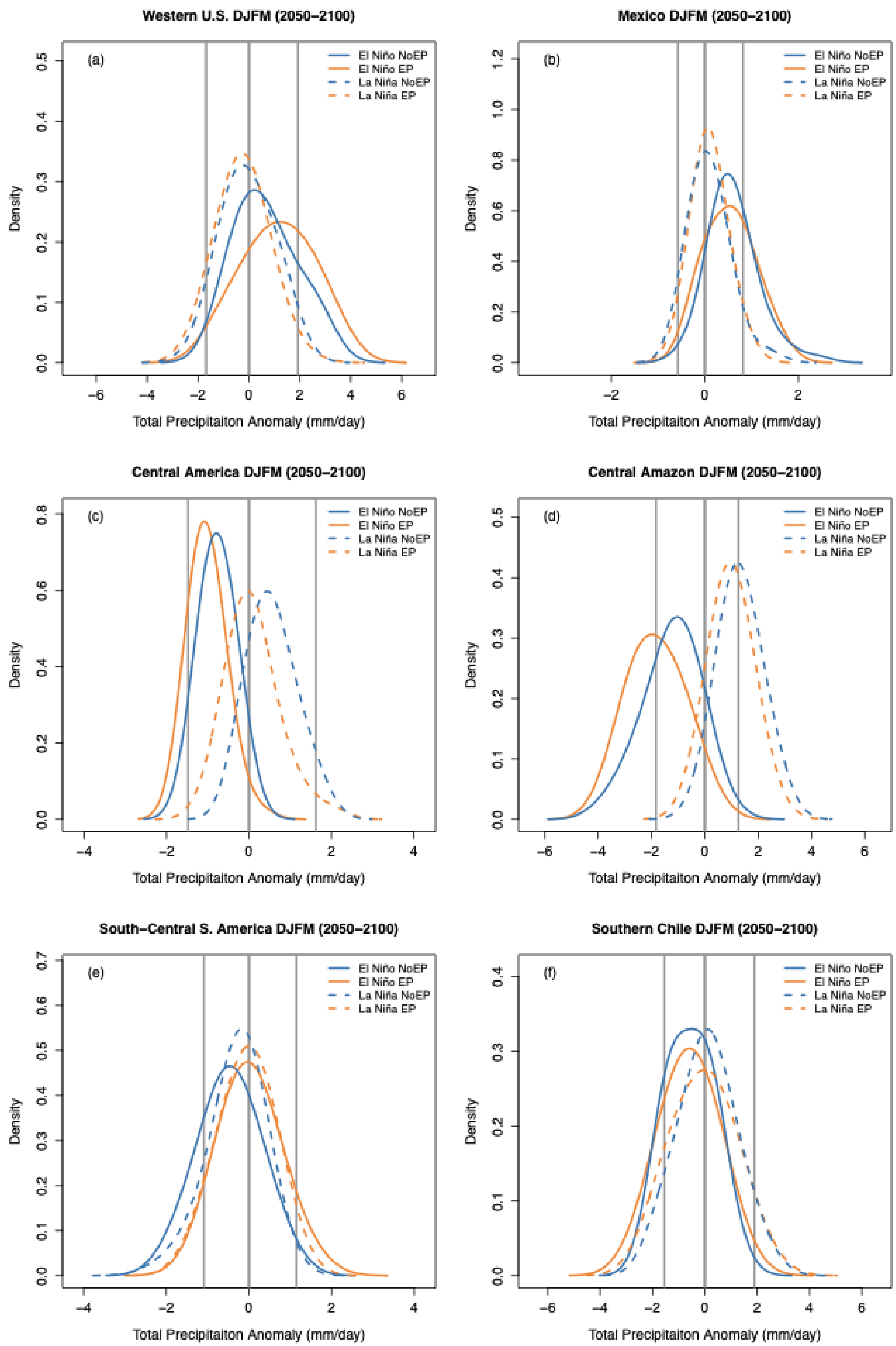

Figure 9. Distribution of boreal winter precipitation anomalies during El Niño and La Nina in the EP and noEP experiments. *Distribution of DJFM precipitation anomalies during 2050-2100 in the EP (orange) and noEP (blue) experiment relative to the Control experiment for El Niño (solid curves) and La Nina (dashed curves). The vertical grey lines indicate the mean, 2.5^{th} and 97.5^{th} percentiles of the Control experiment.*